

Quantification of heat losses through building envelope thermal bridges influenced by wind velocity using the outdoor infrared thermography technique



Małgorzata O'Grady^a, Agnieszka A. Lechowska^b, Annette M. Harte^{a,*}

^a Civil Engineering, College of Engineering and Informatics, National University of Ireland Galway, Galway, Ireland

^b Department of Environmental Engineering, Cracow University of Technology, Cracow, Poland

HIGHLIGHTS

- A method to assess thermal bridging heat loss using the outdoor ITT is developed.
- The ITT approach is compared with hot box measurements and numerical predictions.
- The wind velocity impact on thermal bridging is quantified.
- Adjusting procedure for the Ψ -value measured at different wind velocities is developed.
- This procedure allows measured and standard Ψ -value comparison.

ARTICLE INFO

Keywords:

Building envelope
Hot box
Forced convection
Infrared thermography technique
Quantitative thermography
Thermal bridging

ABSTRACT

Improving the thermal performance of the existing building stock is essential to significantly reduce the overall energy consumption in the building sector. A key objective is the retrofitting of the existing building envelope. A necessary first step in the building envelope optimization process is the assessment of its actual thermal performance. This assessment should be repeated after retrofitting to clearly define the improvements that were made and the heat loss reduction that was achieved. In this study, an efficient, non-destructive, in-situ measurement method, based on an outdoor infrared thermographic survey, is developed to determine the thermal bridging performance. As wind velocity significantly influences the heat losses through the building envelope, this study includes quantification of the wind velocity impact on the Ψ -value. This was assessed by undertaking ITT of the same thermal bridge at various wind velocities, in a controlled environment, in a hot box device. The results showed that the Ψ -value is highly dependent on wind velocity so that measurement of the Ψ -value taken at different wind conditions cannot be directly compared. An adjustment procedure is proposed that can be used to convert the Ψ -value measured at any wind velocity to a standard value corresponding to a velocity of 4 m/s. From a practical point of view, this adjustment procedure makes the methodology widely applicable.

1. Introduction

It is estimated that energy related to buildings is responsible for 40% of total EU energy consumption. To achieve the EU 2030 energy and climate goals, it is essential to limit building-related energy. The European Union Directive 2010/31/EU on Energy Performance of Buildings (EPBD) [1] obliged the EU Member States to implement changes in national building regulations. These changes include setting strict minimum requirements on building energy performance and introducing a national building energy certification system. In November 2016, the European Commission evaluated the effectiveness and

relevance of this directive [2]. They found that combining minimum standards requirements on building energy performance and its certification works effectively particularly with respect to newly constructed buildings. However, large opportunities for savings are still not being harnessed. These concern the existing building stock which has been retrofitted but at a substantially slow pace. Based on this evaluation, a proposal for amending the EPBD [3] has been issued. Its key objective is to fast-track the retrofitting of existing buildings, particularly those with poorest performance. The importance of this issue is further supported by the fact that about 75% of existing buildings are energy inefficient and only 0.4–1.2% of these buildings, depending on Member

* Corresponding author.

E-mail address: annette.harte@nuigalway.ie (A.M. Harte).

Nomenclature

a, b, c	coefficients of Eqs. (3) and (4), –
d, e, f, g	coefficients of Eqs. (20) and (22), –
ϵ	surface emissivity, –
h	heat transfer coefficient, W/(m ² K)
H	specimen height, m
l	length, m
L	specimen length, m
k	thermal conductivity, W/(m ² K)
ν	kinematic viscosity, m ² /s
N	number of pixels on IR line, –
Nu	Nusselt number, –
Pr	Prandtl number, –
q	heat flow rate per unit height, W/m
\dot{q}	surface heat flux, W/m ²
\dot{Q}	heat flow rate (through the specimen), W
R	thermal resistance, m ² K/W
RD	relative percentage deviation, %
Re	Reynolds number, –
σ	Stefan-Boltzmann constant, W/(m ² K ⁴)
T	temperature, °C
U	overall heat transfer coefficient, W/(m ² K)
w	air velocity, m/s

Ψ	linear thermal transmittance, W/(m K)
ρ	density, kg/(m ³)

Subscripts

adj	adjusted
c	convective
ch	characteristic
b	baffle
e	cold side, external conditions
i	hot side, indoor conditions,
$meas$	measured
min	minimum
n	environmental
$plain$	component without thermal bridge
r	radiative
s	surface
S	standard
sp	specimen
sur	surrounding
TB	thermal bridge
tot	total
u	uniform
x	pixel

State, are retrofitted annually.

In answer to this substantial problem, a significant number of research projects have focused on optimization of the building' energy performance. These have demonstrated different approaches for achieving the most energy efficient solution when constructing a new building or renovating an existing one [4–8]. The optimization tools developed consider a range of criteria including, inter alia, primary energy consumption, thermal comfort, investment cost and environmental impact. One of the most effective measures in optimizing building energy efficiency is upgrading the thermal performance of the building envelope. The building envelope provides a thermal barrier between the indoor and outdoor environments, and its standard determines a building's energy requirements. It is clear that the more heat that escapes via an external envelope, the more heat that has to be produced for the comfort of the users. Therefore, heat losses through the building envelope should be eliminated or at least limited [9]. Many researchers have focused on this important aspect by developing computer models for improving its design [10–13]. Variables considered in these models include thermal properties and thickness of the building envelope, external and internal shading systems, and glazing area.

To prioritise existing buildings for retrofitting and to optimize the retrofitting strategy, it is necessary to assess their current thermal performance. Heat loss via the building envelope can be considered to comprise two components: heat lost through the plain parts, described by the thermal transmittance (U -value) and heat loss via thermal bridging. A thermal bridge is a part of the building envelope which has lower thermal resistance due to different geometry, conductivity or fabric thickness, and this can significantly impact on the overall thermal standard of the building envelope and the energy efficiency of a building. The thermal bridging heat loss through a linear thermal bridge is usually quantified in terms of a linear thermal transmittance (Ψ -value), which is the steady state heat flow rate per unit length of bridge per unit temperature difference between the indoor and outdoor environments. Default Ψ -values for standard building details can be found in ISO 14683 [14] though their typical accuracy varies between 0% and 50% [14]. More accurate Ψ -values ($\pm 5\%$) can be obtained from numerical calculations [14]; however, this requires a detailed knowledge of the internal structure of the building envelope together with the properties of the component parts, which may have deteriorated with

time. This requirement makes the numerical approach unsuitable for many existing buildings. In this case, the thermal bridging heat loss should be measured in-situ. This requires the development and implementation of non-destructive assessment tools.

The infrared thermography technique (ITT) may be used as a non-invasive method of measuring the building thermal performance. Thermal images provide detailed information about the internal or external surface temperature distribution, and this has been used by a number of researchers to quantify the thermal performance. Kylili et al. [15] reviewed applications of ITT for building diagnostics. To date, most of the work has focussed on the determination of the U -value of plain building components and a limited number of researchers [16–19] have applied the ITT to quantifying the Ψ -value. Benkő [16] used the outdoor ITT on site and expressed the heat loss associated with thermal bridging as a ratio that reflects the increase of heat loss in the presence of a thermal bridge. A similar approach was presented by Asdrubali et al. [17] who used indoor ITT for a laboratory-based study. To fully quantify the heat loss caused by thermal bridges, they multiplied the experimentally-determined ratio by the U -value of the plain element measured by a heat flow meter (HFM). For both studies, the surface heat transfer coefficient was treated as a constant value along the whole area of the thermogram. Bianchi et al. [18] validated the Asdrubali methodology on a full-scale building and, as the construction of the building envelope was known, they calculated the U -value, instead of measuring it with a HFM. O'Grady et al. [19] developed a methodology of quantifying the Ψ -value by means of the indoor ITT solely. This methodology considers the convective and radiative coefficients correlated with surface temperatures. Therefore, these coefficients were evaluated for the whole range of temperatures recorded in the infrared image (IR image). This approach improved the accuracy significantly and was validated in a hot box device. It is usually easier to control the environmental conditions for ITT inside a building than outside. Additionally, as reported by Fox et al. [20], indoor ITT is more suitable to visualize building envelope defects, such as service faults, ventilation, moisture or conductivity discontinuation. However, for an occupied building, it may not be possible to undertake the indoor thermographic survey and, in that case, outdoor ITT is the only option.

The quantitative outdoor infrared thermography technique (ITT) is based on the surface energy balance principle applied to the external

surface of the building envelope, and it is influenced significantly by weather conditions. Over the past number of years, researchers have aimed to define the impact that these parameters have on the outdoor ITT and to establish the most suitable weather conditions for it. Some weather factors, such as rain [21] or solar irradiation [21,22] should be always avoided during the outdoor thermography survey. Lehman et al. [23] simulated the influence of the solar irradiation on six building walls with different internal structures. Simulations revealed that the increase in wall surface temperatures depends on the thermal mass of the wall so the waiting period for the influence of solar irradiation to dissipate before performing ITT is dependent on the wall structure. In order to avoid direct sunlight, Albatici and Tonelli [24] recommended evenings and early mornings as the most suitable times for the outdoor ITT. Lehman et al. [23] and Albatici et al. [21] recommended undertaking the thermographic survey with a fully overcast sky in order to achieve a sky temperature similar to the air temperature and thus minimize radiative heat losses of the building element to the sky. Considering the difference between the indoor and outdoor air temperatures for the thermographic survey, various recommendations have been found. According to infrared camera manufacturers' FLIR manual [25] and to Fokaides and Kalogirou [26], it is important to have a minimum temperature difference of 10 °C between inside and outside. Other manufacturers [27] recommend a 15 °C difference between the indoor and outdoor air temperature. Albatici et al. [21] suggest a minimum of 10 °C, and preferably at least 15 °C.

Many researchers have aimed to define the wind speed limit for accurate outdoor thermographic survey. Lehman et al. [23] suggested that pulsating wind up to 2 m/s has a negligible influence on the thermography and showed that surface temperature disturbances caused by the wind decay within a few hours. According to Balaras and Argiriou [28] and Albatici et al. [21], external surveys should be avoided under windy conditions, (exceeding 5 m/s). Additionally, Albatici et al. [21] recommended that the hourly average of free stream wind in the building vicinity within 24 h should be below this limit.

This paper presents a methodology for characterizing the Ψ -value of building components using outdoor ITT. The approach is an adaptation of the methodology developed for indoor ITT described in [19] and accounts for the influence of wind velocity on the external surface temperatures. The methodology is developed using experimental and numerical approaches. The experimental study is carried out in laboratory conditions in a hot box device. This arrangement allows for isolation of the wind effect by keeping the indoor and outdoor air temperatures at the same level throughout testing and by eliminating the effect of solar irradiation. Using infrared images, the wind impact on heat loss through both thermal bridging and uniform wall components at different wind velocities is observed. To evaluate the Ψ -value, the external convective heat transfer coefficients (h_{ce}) are also required and different approaches to their evaluation are investigated. Ψ -values evaluated by means of outdoor ITT are validated against those obtained using the hot box measurement method [29].

Numerical modelling is undertaken to evaluate the standard Ψ -value in accordance with EN ISO 10211 [30] using two-dimensional heat transfer finite element models. This Ψ -value is evaluated using standard boundary conditions and specifically using external convective coefficient corresponding to a wind velocity of 4 m/s, in accordance to EN ISO 6946 [31]. To compare the in-situ thermal bridge performance to the standard value, measurements should be carried out at this exact wind speed. As it is considered very restrictive to undertake in-situ measurements only at this wind velocity, an approach is developed that can account for different wind conditions. In this work, numerical models are developed for a wide range of wind velocities and used to develop adjustment factors to convert the Ψ -value at a non-standard wind velocity to the standard value. These adjustment factors are then validated against the experimental values.

2. Different approaches to accounting for wind effects on a building external surface

The external surface of a building continually interacts with the surrounding environment via thermal radiation and convection. Thermal radiation includes the energy that is emitted and absorbed by an external building surface to or from the surroundings. Convection is the interaction between the building and moving air and is dependent on the temperature difference between the surface and air, the speed and the direction of wind, and also the geometry and coarseness of the surface. It occurs in two modes at the surface, namely, free convection and forced convection. Free convection involves air flow movement that is caused by buoyancy forces as a result of changes in air density near the building surface. Forced convection describes air movement that is induced in a natural environment by wind [32,33]. This mode predominates in outdoor conditions, where wind strongly influences heat losses from building envelope surfaces.

The interaction between the outdoor environment and the building is described using the external surface heat transfer coefficient h_e that includes radiative and convective components. Evaluation of these coefficients is necessary in order to define external boundary conditions of a building envelope surface. These boundary conditions may then be implemented in heat transfer analytical and computing simulations, or in calculations from in-situ measurements, such as outdoor ITT. The radiative coefficient h_{re} is not directly influenced by the wind velocity and can be found from Eq. (1):

$$h_{re} = \varepsilon\sigma(T_s + T_e)(T_s^2 + T_e^2) \quad (1)$$

where ε is the surface emissivity, σ is the Stefan-Boltzmann constant and T_s and T_e are the surface and air temperatures, respectively.

According to well-established heat transfer theory [32], several features should be taken into account when determining the value of the convective coefficient h_{ce} . Such features include the shape of the surface, the flow conditions (laminar or turbulent) and the physical properties of the air. Calculating the external heat transfer convective coefficient from Eq. (2) takes all these aspects into account:

$$h_{ce} = \frac{Nu k}{l_{ch}} \quad (2)$$

where Nu is the Nusselt Number, which is dependent on the type and conditions of flow, k is the thermal conductivity of air and l_{ch} is the characteristic length over which h_{ce} applies.

Thermal and hydrodynamic boundary layers are formed around building surfaces exposed to air temperatures (different to surface temperatures) and to the wind motion, respectively. A building component interacts with the air in these boundary regions. A thermal boundary layer is a region where the air temperature changes from the surface temperature into the free stream air temperature. A hydrodynamic boundary is a thin air layer in which the wind velocity changes from 0 m/s at the surface to the free stream velocity at some distance from the surface. Within this hydrodynamic boundary layer, the wind flows at a local velocity.

Different approaches to calculating the external convective coefficient have been developed. Researchers have aimed to produce accurate predictions, while simultaneously simplifying the specific calculations required. The first researchers to develop an approximation of relationship between h_{ce} and the wind velocity were Nusselt and Jürges [34]. Their approximation was based on a wind tunnel experiment investigating parallel flow over a flat plate. They suggested that the convective coefficient could be calculated from linear interpolation for wind velocities lower than 5 m/s and using a power law for higher wind velocities. Those two scenarios can be written as Eqs. (3) and (4), respectively, and are known as Jürges' equations.

$$h_{ce} = a + bw \quad w < 5 \text{ m/s} \quad (3)$$

$$h_{ce} = cw^{0.78} \quad w \geq 5 \text{ m/s} \quad (4)$$

where w is the wind speed in m/s and constants a , b and c are given in Table 1. Cole and Sturrock [35] confirmed that Eq. (3) includes a radiative component. This component is omitted while the approximating convective coefficient for higher wind velocities using Eq. (4) [36].

McAdams [37] published a recast of these empirical equations with slightly different constants, also given in Table 1, and since then the recast versions have been widely used. Palyvos [36] undertook a comprehensive comparison of different approaches to calculating the value of convection coefficients by surveying more than fifty correlations available in the literature. Emmel et al. [39] showed that convective coefficients strongly affect the result of thermal simulations and should, therefore, be applied precisely to fully describe the wind conditions. Sartori [40] investigated the relative accuracy of the different approaches and found that the convective coefficients calculated using the Nusselt correlations tend to be the most accurate as only this approach takes into account the distinction between laminar and turbulent flow and the characteristic length over which the convective coefficient is applied. This characteristic length corresponds to the real path of the wind over the surface and it can have a significant influence on the values of the convective coefficient for the surface considered. They showed that the coefficients calculated for turbulent and for laminar flow decrease with an increase in characteristic length, which is in agreement with the boundary layer theory.

Evaluation of the external heat transfer coefficients is an important step in the evaluation of building envelope performance using the outdoor ITT. Researchers who evaluated U -values of homogeneous building elements by means of the outdoor ITT evaluated surface heat transfer coefficients various ways. Albatici et al. [21] described h_{ce} using a modified Jürges' equation with the constants presented in Table 1. However, they simplified this to Eq. (5) and applied the Stefan-Boltzmann law to express the radiative component. Their U -value formula, described by Eq. (6), is valid for wind velocity lower than 5 m/s.

$$h_{ce} = 3.8054w \quad (5)$$

$$U = \frac{5.67\varepsilon \left[\left(\frac{T_s}{100} \right)^4 - \left(\frac{T_e}{100} \right)^4 \right] + 3.8054w(T_s - T_e)}{T_i - T_e} \quad w < 5 \text{ m/s} \quad (6)$$

Albatici et al. [21] used this methodology to assess five different light-weight and heavy external walls of an experimental building. The U -values calculated for heavy walls using the ITT showed absolute deviations of 8–20% when compared to the U -values obtained from HFM, and around 20% in comparison to the theoretically calculated U -values. However, the U -values of light-weight walls using the ITT had absolute deviations of around 30–40% compared with other methods and it was concluded that further work on developing the ITT methodology for light-weight and well-insulated walls was necessary. Similarly, Dall'O' et al. [38], used Jürges equation for evaluating the external heat transfer coefficient when evaluating the U -value by means of the outdoor ITT of fourteen heavy and light structure walls in existing buildings. U -values of these building walls, situated in suburban areas and exposed to a wind speed of 1 m/s, showed a percentage deviation of –40% to +60% between the theoretical and the measured U -values using this methodology. As a much higher deviation of between –70% and +105% was found for externally insulated walls situated in the urbanized area exposed to a wind speed of 0 m/s, the method was deemed unsuitable for these types of walls.

The ISO 6946 [31] defines the standard boundary conditions that may be applied to numerical simulation, in the absence of detailed information on the boundary conditions. These conditions were evaluated for wind velocity of 4 m/s and, in practice, are widely used. The same standard provides a calculation procedure for specific boundary conditions, where the external convective coefficient h_{ce} can be obtained from Eq. (7). This equation can be applied for any wind velocity:

$$h_{ce} = 4 + 4w \quad (7)$$

In the following sections, the influence of these different approaches to evaluating the external heat transfer coefficient is considered in detail.

3. Experimental study

An experimental study was undertaken to assess the thermal response of building envelope components exposed to different wind velocities. To eliminate the impact of other weather factors on the thermal behaviour of the tested building components, the experimental study was conducted in a controlled laboratory environment using a hot box device [29]. Hot box measurements of heat flow rate through components containing thermal bridges were carried out at three different wind velocities. IR images were then taken while the specimens were still mounted in the device immediately after completion of hot box measurements. This allowed for assessment of the suitability of a proposed external ITT methodology under variable external wind exposures.

3.1. Experimental set up

The experiment in the hot box device (as shown in Fig. 1) was designed to evaluate heat losses through thermal bridging situated in building envelope components for free stream wind velocities between 0.5 m/s and 4 m/s. The device comprises two chambers: the guarding box (hot side) represents indoor conditions while the climatic box (cold side) simulates the outdoor conditions. Tested specimens were placed successively into a surround panel. To control the environmental conditions close to the exposed faces of the specimen, baffles were mounted around the specimen on both sides. In order to simulate free convection conditions on the hot side and to ensure that the specimen was exposed to a uniform air temperature, the air within the baffle had a uniform velocity of 0.1 m/s. The cold baffle was fastened to the cold surface of surround panel. The heat flow rate through each specimen was measured with the metering box and the air temperature and wind velocity between the baffles and specimen were continually monitored during the tests.

On completion of the hot box testing, the cold baffle was replaced with a new wind baffle, made of plywood, with holes to accommodate the IR camera. This was necessary because, when the original cold baffle was removed from the specimen to take the IR images, the wind changed its speed and direction. With this new baffle, it was possible to take the images under the controlled wind conditions.

3.2. Geometries and description of the specimens

Two specimens containing thermal bridges and a third plain specimen were tested. The specimens were made of structural insulated panels (SIP) comprising 100 mm thick low conductivity extruded polystyrene insulation (XPS) boards and 15 mm thick oriented strand-board (OSB) sheathing on each side. All specimens were 1.5 m long, 1.5 m high and had a thickness of 130 mm. Specimen 1, presented in Fig. 2, is a SIP panel containing a steel square hollow section (SHS) of dimensions 100 × 100 × 5 mm, filled with XPS. This specimen represents a thermal bridge created by a steel column, often used as a structural member of a building external envelope.

Table 1
Constants a , b and c for Eqs. (3) and (4).

Constants	Nusselt and Jürges [34]	McAdams [37]	Albatici et al. [21] Dall'O' et al. [38]
a	5.8	5.7	0
b	4.1	3.8	3.8054
c	7.3	7.2	–

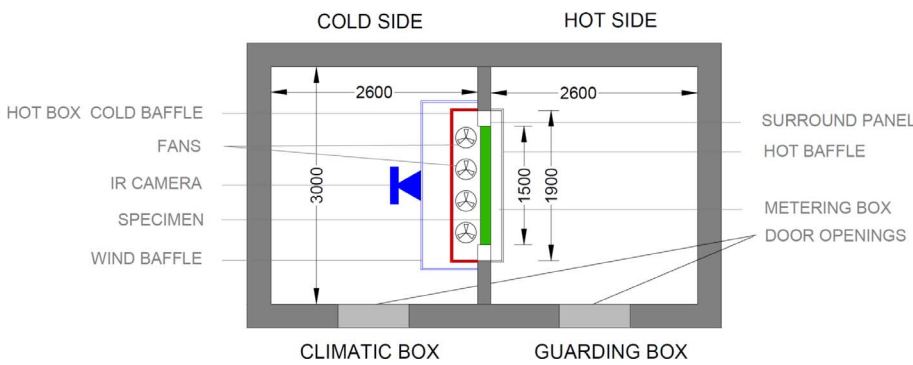


Fig. 1. Experimental set up (dimensions in mm).

Specimen 2, shown in Fig. 3, is a SIP panel with two steel square hollow sections (SHS) filled with XPS (dimensions 100 × 100 × 5 mm). This specimen represents adjacent thermal bridges situated about 50mm apart.

Specimen 3, without thermal bridging, was tested in order to allow for the determination of the Ψ -value for Specimens 1 and 2.

3.3. Hot box testing

The three specimens, described in the previous section were tested in accordance to the EN ISO 8990 [29] standard. For these tests, different uniform wind velocities were induced between the cold baffle (marked in red in Fig. 1) and the specimen surface. For each specimen, tests were carried out at three different wind velocities: 0.5 m/s, 1.5 m/s and 4 m/s. As the wind velocities were average values measured over a period of time, it was not possible to control the wind conditions to achieve these exact values; the average values for each test are reported in Table 2, together with their standard deviations. The wind velocity was measured every two minutes, at mid-height and midway between the specimen surface and the cold baffle, using thermoanemometers INT 512 having a measurement range of 0.2–10 m/s. The air temperatures during all the tests were kept at the same level, around +25 °C on hot and –5 °C on the cold side.

In Table 2, environmental temperatures on the hot side (T_{ni}) were obtained as a weighting of hot air temperatures recorded during testing (T_i) and hot baffle surface temperatures ($T_{si,b}$). Similarly, the environmental temperatures on the cold side (T_{ne}) were obtained as a weighting of cold air temperatures (T_e) and a cold baffle surface temperatures ($T_{se,b}$). This was undertaken to meet requirements of EN ISO 8990 [29] and ISO 12567-1 [42]. These standards state that for calculations based on heat flow rate measured in a hot box (such as Ψ -value), an environmental temperature T_n should be used. The full procedure of obtaining the environmental temperature T_n is presented in [19].

Testing started with the insertion of Specimen 1 into the hot box device. A wind velocity of around 0.5 m/s for the first case was created by adjusting the power of the fans installed above the cold baffle. This arrangement created an upward wind. Once the desired wind velocity was achieved, the power of the vents was kept at the same level.

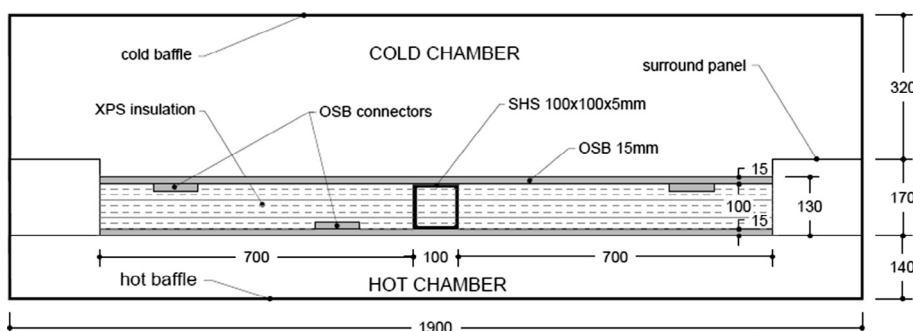


Fig. 2. Cross-section of Specimen 1 inserted into hot box.

Concurrently, the conditions in the hot chamber were set to allow for free convection with a wind velocity of 0.1 m/s directed downward. The required wind velocity and air temperatures in each chamber were kept fixed for a period of a few hours from the moment when a steady state had been reached. The measurements taken facilitated the calculation of the heat flow rate through the specimen \dot{Q}_{sp} . This procedure was repeated for the higher wind velocities of about 1.5 m/s and 4 m/s.

To assess the thermal bridging heat loss q_{TB} using the hot box, the heat flow rate through an identical plain specimen \dot{Q}_{plain} at similar wind velocity is required. The thermal bridging heat rate q_{TB} represents the additional heat loss through the specimen caused by presence of the linear thermal bridge per unit length of the thermal bridge.

Having values of heat flow rate for all specimens, q_{TB} is obtained from Eq. (8) and finally the Ψ -value from Eq. (9):

$$q_{TB} = \frac{\dot{Q}_{sp} - \dot{Q}_{plain}}{H} \quad (8)$$

$$\Psi = \frac{q_{TB}}{T_{ni} - T_{ne}} \quad (9)$$

This procedure was repeated for Specimen 2. \dot{Q}_{plain} for Specimen 3 was measured in the hot box device in similar conditions to Case 2. For other cases, the heat flow rates were derived from CFD simulations.

3.4. ITT testing

In this part of the experiment, the heat loss via thermal bridging at different wind velocities was assessed by means of the outdoor ITT. In this case, the heat loss was calculated using the surface temperatures on the cold side of the specimen recorded during a thermographic survey. The aim was to carry out all ITT tests under the same conditions as the hot box testing. However, the replacement of the original cold baffle with the new wind baffle (marked in blue in Fig. 1) made the control of the air temperature to –5 °C not possible. The air temperature in this chamber T_e was measured during tests. The wind velocity for each of the ITT tests was kept at a comparable level to that in the hot box tests. Table 3 presents conditions for both specimens for the ITT testing.

Similarly to the hot box testing, the required wind velocity for each case was induced by adjusting the power of the vents installed above

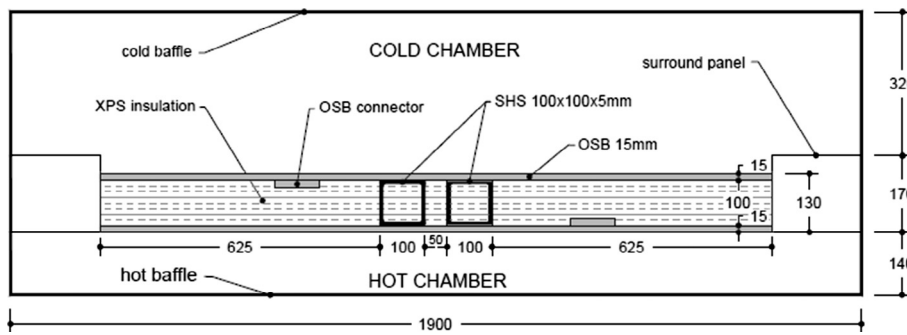


Fig. 3. Cross-section of Specimen 2 inserted into hot box.

Table 2
Conditions for hot box testing of Specimen 1 and Specimen 2.

		Specimen 1			Specimen 2		
		Case 1	Case 2	Case3	Case 1	Case 2	Case3
w_e	m/s	0.52	1.43	4.35	0.52	1.54	4.35
$SD w_e$	m/s	0.06	0.12	0.13	0.06	0.07	0.13
w_i	m/s	0.1	0.1	0.1	0.1	0.1	0.1
T_e	°C	-4.88	-4.90	-5.14	-4.66	-4.85	-5.17
T_i	°C	24.77	24.73	24.74	24.66	24.67	24.67
$T_{se,b}$	°C	-4.89	-4.94	-5.18	-4.69	24.67	-5.20
$T_{st,b}$	°C	24.25	24.24	24.25	24.05	24.02	24.00
T_{ne}	°C	-4.89	-4.92	-5.18	-4.69	-4.87	-5.20
T_{ni}	°C	24.41	24.39	24.40	24.24	24.23	24.21

Table 3
Conditions for the ITT testing of Specimen 1 and Specimen 2.

		Specimen 1			Specimen 2		
		Case 1	Case 2	Case3	Case 1	Case 2	Case3
w_e	m/s	0.47	1.57	4.27	0.58	1.54	4.18
w_i	m/s	0.1	0.1	0.1	0.1	0.1	0.1
T_e	°C	-7.2	-7.2	-7.3	-7.0	-6.5	-6.9
T_i	°C	24.89	24.74	25.01	24.64	24.61	24.65

the cold baffle. After a steady state with the desired wind velocity and temperature established, the ITT was performed. This procedure was repeated for all test cases. Due to the fact the recorded temperatures by the IR camera oscillate even when captured under the steady conditions, a series of IR images of Specimen 1 and Specimen 2 were taken at each wind velocity. From each IR image, three horizontal rows of pixels at mid-height were extracted. The measured temperatures of these rows were used to create an IR line, which represents the temperature variation along the specimen. A typical IR image, with an IR line is shown in Fig. 4. To smooth the transition of surface temperatures from one pixel to the next one, each pixel on the IR line represents the mean temperature of the middle line pixel and its eight neighbouring pixels. This IR line shows fully the surface temperature disturbance caused by the vertical thermal bridge. Then from all these IR lines for each case, a mean IR line was created. As the specimens were symmetrical, it was only necessary to create IR lines for half of the specimen. Fig. 5 shows the IR lines from each image together with the mean IR line for one of the tests. The thermal bridge presented on this figure is caused by a steel column in a structural insulated panel (SIP) and its geometry is shown in Fig. 2.

The horizontal field of view represents the length of the object captured by an IR camera and it depends on the camera resolution and on the distance between the camera and the surface. Throughout this experiment, the distance at which IR images were taken was dictated by the construction of the wind baffle. The IR camera used in this experiment, a FLIR T335 with resolution 320 × 480, was equipped with

25° lens. As the length of each IR image was 0.314 m, it was necessary to use more than one image to capture the full region influenced by the thermal bridge. Merging of IR lines produced from these images was then carried out. This is seen in Fig. 5, where merging occurs at a specimen length of around 0.60 m.

4. Outdoor ITT methodology

The mean IR line was used to calculate the Ψ -value using a methodology similar to that reported by the authors for indoor ITT [19] but adapted to account for outdoor boundary conditions. It was assumed that, for a vertical thermal bridge, a horizontal line in the mid-height of the thermogram is sufficient to represent the average temperature distribution caused by the tested thermal bridge [19]. These temperatures were also the most distant from the connection with surround panel on the top and on the bottom of the specimen that may cause some additional disturbances. In reality, other factors could additionally disturb the thermogram, such as screw fixing or furniture and it is important to eliminate them while calculating Ψ -value. This is achieved by creating an IR line where thermal bridge influence can be clearly seen and where it is not perturbed by other factors. In forced convection, the wind velocity varies along the vertical direction. The IR line created at mid-height of the specimen or, in practice, of the building element, shows the temperature distribution impacted by the averaged wind conditions. Such a simplification was necessary while developing a practical method that can be implemented on site in real buildings. The methodology enables quantification of the heat loss associated with the presence of a thermal bridge using only ITT. It is based on the surface energy balance applied to the outdoor building envelope surface. According to this balance, the heat flow rate for each pixel (q_x) on the IR line is found using Eq. (10):

$$q_x = l_x [(h_{cx} + h_{rx}) |T_e - T_{sx}|] \tag{10}$$

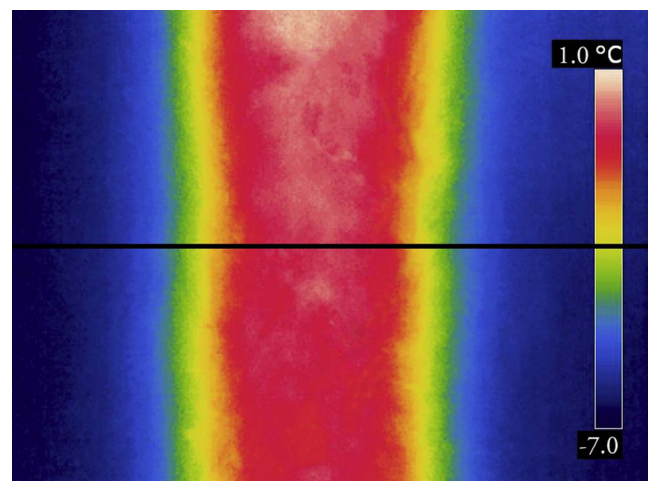


Fig. 4. A sample of an infrared camera image of Specimen 1, Case 2.

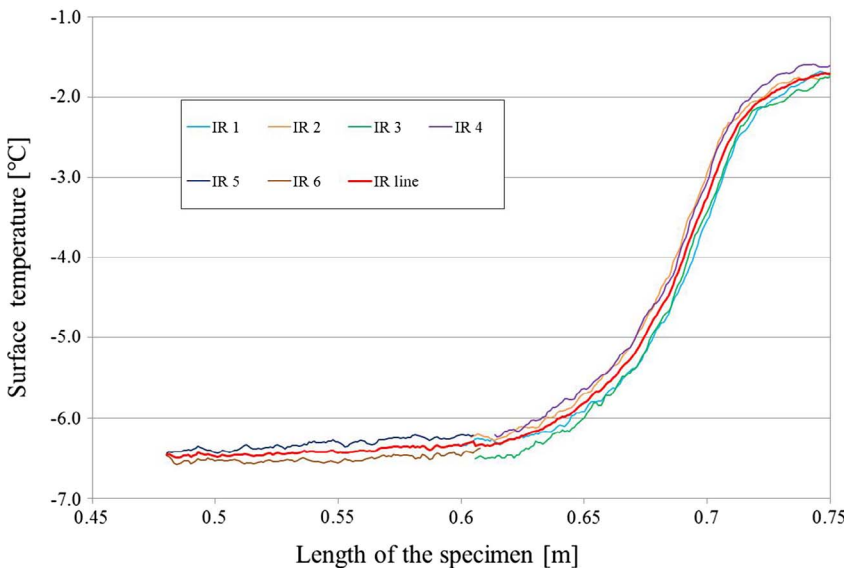


Fig. 5. Mean IR line created from a series of thermograms of Specimen 1, Case 2.

Similarly, by calculating q_{xu} for a pixel outside the thermal bridge zone of influence using Eq. (10) and multiplying it by the number of pixels on the IR line, the heat flow rate through an identical building component with no thermal bridge can be predicted. The thermal bridge heat flow rate for each pixel q_{xTB} can then be found using Eq. (11):

$$q_{xTB} = q_x - q_{xu} \quad (11)$$

By summing up q_{xTB} for all pixels on the IR line, the thermal bridge heat flow rate q_{TB} is found:

$$q_{TB} = \sum q_{xTB} \quad (12)$$

Finally, by dividing this thermal bridge heat flow rate q_{TB} by the temperature difference between the indoor and outdoor environments, the Ψ -value is determined.

$$\Psi = \frac{q_{TB}}{T_i - T_e} \quad (13)$$

In order to quantify the heat flow rate for each pixel q_x using Eq. (10), the convective and radiative heat transfer coefficients must be determined. Since the methodology is developed for outdoor ITT use, the external convective coefficient h_{ce} for forced convection is used. Two approaches to calculating these coefficients are investigated: using heat transfer theory by means of Nusselt number and using Jürges' equation.

4.1. Evaluating heat transfer coefficients using heat transfer theory

The convective coefficient is determined by applying Eq. (2) to each pixel:

$$h_{ce} = \frac{Nu_x k_x}{l_{ch}} \quad (14)$$

The Nusselt number (Nu) is a function of the Reynolds (Re) and Prandtl (Pr) numbers in forced convection.

With forced convection, two types of flow conditions can be distinguished, namely, laminar and turbulent flow. Flow induced by wind over a flat surface is first dispersed from the edge in a laminar mode and this subsequently transforms into turbulent flow. These boundary layer flows are characterized by Reynolds number, which is expressed as the ratio of the inertia to viscous forces:

$$Re_x = \frac{wl_{ch}}{v_x} \quad (15)$$

Conventionally, the transition from laminar to turbulent flow occurs at the location for which the critical Reynolds number is 5×10^5 .

However, the transition can occur at different locations as influenced by roughness of the surface and/or disturbances of the flow. When the flow is induced artificially, by fluid machines such as fans, compressor or pumps, fully turbulent flow takes place along the entire surface [32].

As the relationship between the Nusselt number and the Reynolds and Prandtl numbers depends on the flow conditions, it is described differently for laminar and turbulent flow. The Nusselt number correlations presented by Eqs. (16)–(18) were developed for parallel flow over the surface of a flat plate. However, Rowley and Eckley [41] found experimentally that there was an insignificant reduction in the convection coefficient as the angle between the surface and the wind stream was increased from 15° to 90° . Therefore, Eqs. (16)–(18) can be also applied to characterize flow in a direction other than parallel to external building component surface.

For laminar flow, the Nusselt number is calculated using Eq. (16):

$$Nu_x = 0.664 Re_x^{1/2} Pr^{1/3} \quad (16)$$

A correlation that accounts for mixed flow, in the transition from laminar to turbulent flow, is expressed in Eq. (17). This equation should be used while evaluating the Nusselt number for real outdoor environments in the absence of any disturbances of the flow along the surface of the surveyed building component:

$$Nu_x = (0.037 Re_x^{4/5} - 871) Pr^{1/3} \quad (17)$$

However, if the flow is disturbed, for example by a tree branch, an electric wire or by the surface roughness, it tends to be fully turbulent over the whole length [40]. In this case, the Nusselt number should be evaluated from the correlation expressed by Eq. (18) that accounts for turbulent flow conditions. This equation is used in the analysis covered in this study as wind speed in the experiment was created by fans resulting in fully turbulent flow:

$$Nu_x = 0.037 Re_x^{4/5} Pr^{1/3} \quad (18)$$

The external radiative coefficient h_{re} is calculated for each pixel on the IR line using Eq. (19):

$$h_{rx} = \varepsilon \sigma (T_{sx} + T_e)(T_{sx}^2 + T_e^2) \quad (19)$$

4.2. Determination of heat transfer coefficients for test specimens

As seen in Eq. (14), the convective coefficient is a function of the Nusselt number, air conductivity k , and characteristic length l_{ch} . For the tests specimens in the hot box, the characteristic length is constant and

equal to the specimen height. As the Prandtl number is also constant, the changes in Nusselt number are a function of the Reynolds number, which depends on the wind velocity w and the kinematic viscosity ν . Since the wind velocity can be assumed to be the same along the whole length of the specimen, it can be deduced that the air conductivity k and the kinematic viscosity ν are the only factors which cause a variation in the convective coefficient calculated for each pixel of the IR line. These properties are evaluated at a film temperature, which is the arithmetic mean of the surface temperature of the pixel and the air temperature. Table 4 presents the average convective coefficients calculated for each of the three cases for Specimen 1 and Specimen 2, for the turbulent flow conditions (Eq. (18)) present during testing. Each case represents a different wind velocity induced along the specimen's cold surface. The average h_{ce} is the arithmetic mean of all convective coefficients on the IR line. The deviations between the minimum value of h_{ce} (on the thermal bridge surface) and the maximum value (on the uniform part of the specimen away from the thermal bridge) are very small and amount for Specimen 1 to 0.02 W/(m² K) for Case 1, 0.04 W/(m² K) for Case 2 and 0.06 W/(m² K) for Case 3. It was found that the Ψ -values determined using the average values of h_{ce} and pixel specific values are equal. This finding contrasts with the case for indoor ITT where it was found that applying a convective coefficient (h_{ci}) evaluated for each pixel was necessary to accurately calculate Ψ -value by means of the indoor ITT [19], under natural convection. In natural convection, the convection coefficient is related to the difference between the surface and the air temperature. Surface temperatures of a component containing thermal bridges varied significantly, therefore variable h_{ci} related to these variances, improved the results accuracy. In the forced convection, wind is the predominant factor in evaluating the convective coefficient, therefore does not change its value at varied surface temperatures.

The strong dependency of h_{ce} on wind velocity is seen in Table 4. For Specimen 1, the average value of h_{ce} increased from 3.16 W/(m² K) to 18.51 W/(m² K) as the wind increased from 0.47 m/s to 4.27 m/s. These coefficients are lower than coefficients calculated using the approximate procedure in accordance with EN ISO 6946 [31], Eq. (7). As mentioned in Section 2, h_{ce} evaluated using Nusselt number tends to be the most accurate as it takes into account, for instance, flow conditions, that is not distinguished in the standard approach.

The average h_{re} was calculated as an arithmetic mean of all radiative coefficients on the IR line. The differences between Ψ -values calculated from average h_{re} and Ψ -values obtained from pixel values of h_{re} are very small and are the order of 1.5%. Therefore, it is reasonable used average radiative coefficients. The average values of h_{re} for each case are given in Table 4 and can be seen to be independent of wind speed.

4.3. Evaluating heat transfer coefficients using Jürges' equation

The second method used to evaluate the external heat transfer coefficient was using Jürges' equations. In this study, only wind velocities up to 5 m/s are implemented; therefore, Eq. (3), with constants provided by McAdams [37], is applied. Sartori [40] compared the relationship between wind velocities up to 5 m/s and convective coefficients expressed by different approximations. He concluded that h_{ce} evaluated by Jürges' equation increases with increasing wind velocity at the same rate as that obtained using the Nusselt correlation for fully turbulent flow (Eq. (18)). Therefore, Jürges' approach is included in this study as an alternative way to characterize turbulent flow. Values of coefficients evaluated using Jürges' equation also account for radiative losses [43] and they are constant along the whole length of the specimen (see Table 5). Table 5 also shows the total average heat transfer coefficient for each case determined by adding the average h_{re} and average h_{ce} values given in Table 4. The maximum difference in the heat transfer coefficients calculated using the two approaches is 5.3%.

5. Experimental results and discussion

In this section, the results obtained from the hot box device and from the ITT survey taken at different wind velocities are presented and discussed. Surface temperature distributions measured by the outdoor ITT are presented and then the heat losses via thermal bridging expressed as linear thermal transmittance Ψ -values for each specimen tested at three different wind velocities are presented.

5.1. Surface temperatures measured by the outdoor ITT

Temperature distributions of each specimen were obtained at different wind velocities. In each case, several thermograms were recorded and a mean IR line representing the horizontal variation of the temperature distribution for each specimen was evaluated. In Fig. 5, IR lines from 6 thermograms and the mean IR line are shown.

Obviously, surface temperatures decrease when exposed to increased wind velocity. Figs. 6 and 7 present surface temperature distributions for the left halves of Specimens 1 and 2 for all three cases. The maximum temperature occurs in the middle of the thermal bridge in both cases. This corresponds to a distance of 0.75 m for Specimen 1 and 0.626 m for Specimen 2. Figs. 6 and 7 clearly demonstrate the correlation between the wind velocity and surface temperatures.

Table 6 gives a summary of the temperatures on the thermal bridge (T_{TB}) and the uniform temperature (T_u) on the plain part of the specimen for each case. The T_{TB} was measured in the middle of the thermal bridge, at distance of 0.75 m for Specimen 1 and 0.675 m for Specimen 2. Both temperatures, T_u and T_{TB} , were measured at the specimens' mid-height. In addition, the standard deviations (SD) for these temperatures are given. The wind velocity has a greater impact on the surface temperatures on the thermal bridge than those on the plain surface. For Specimen 1, the plain temperature, measured at a wind velocity of 1.57 m/s, decreases by 0.46 °C whereas the temperature on the thermal bridge decreases by 1.90 °C when compared to the surface temperatures captured with the wind velocity of 0.47 m/s. Increasing the wind velocity to 4.27 m/s results in a further decrease in the plain temperature of 0.41 °C, compared to 2.14 °C on the thermal bridge. As a result, the difference between the minimum and maximum surface temperatures decreases as the wind velocity increases. This difference for Specimen 1 is 6.17 °C at 0.47 m/s, 4.73 °C at 1.57 m/s and 3.00 °C at 4.27 m/s. A similar trend is seen for Specimen 2.

5.2. Thermal bridge heat loss expressed by linear thermal transmittance Ψ -value

In this section, Ψ -values evaluated by means of outdoor ITT are compared to these measured in the hot box. For the ITT calculations, the external convection coefficient h_{ce} was calculated using the two procedures described above. The Ψ -values calculated using the Nusselt number to obtain the surface heat transfer coefficients are labelled with a subscript Nu and those evaluated using h_{ce} from Jürges' equation, are labelled with subscript Ju .

Though the aim was to perform both the hot box and the ITT testing under exactly the same conditions, the wind velocities varied slightly as they represent average values measured over a period of time. However, as can be seen in Tables 2 and 3, the maximum difference

Table 4
Convective coefficient values calculated using Nusselt correlation (Eq. (18)) and radiative coefficient values.

Parameter	Unit	Specimen 1			Specimen 2		
		Case 1	Case 2	Case3	Case 1	Case 2	Case3
Aver h_{ce}	W/(m ² K)	3.16	8.31	18.50	3.74	8.17	18.17
Aver h_{re}	W/(m ² K)	4.01	3.99	3.98	4.03	4.03	4.00

Table 5
External heat transfer coefficients using Jürges' equation and heat transfer approach Nusselt correlation.

Parameter	Unit	Specimen 1			Specimen 2		
		Case 1	Case 2	Case3	Case 1	Case 2	Case3
Jürges $h_{ce} + h_{re}$	W/(m ² K)	7.49	11.67	21.93	7.90	11.55	21.58
Nusselt $h_{ce} + h_{re}$	W/(m ² K)	7.17	12.30	22.48	7.77	12.20	22.17
Difference	%	4.5	5.1	2.5	1.7	5.3	2.7

between the wind velocities in both tests is 0.17 m/s and can be described as minor. Due to the necessity to change the wind baffle for the ITT tests, the temperature in the cold chamber was different: for the hot box tests this temperature was about -5 °C whereas for the ITT tests it was about -7 °C. The difference in air temperatures between the hot and cold chambers are summarized in Table 7. However, as the Ψ -values are calculated as the quotient of q_{TB} and the difference between the cold and hot air temperatures, values from both test methods can be compared directly.

Ψ -values are presented in Table 8 for each wind velocity. As expected, heat losses via the thermal bridging increase proportionally to the increase in wind velocity along the surface of the specimens. In Case 1 for both specimens, the ITT and the hot box measured the smallest Ψ -value compared to other cases. In this case, relative deviations (RD) between Ψ_{Nu} -values amounted to -9% for Specimen 1 and -6% for Specimen 2, in contrast to hot box measurements. Ψ_{Jur} -values represent RD of -5% for both specimens. For Case 2, representing a higher wind velocity, the Ψ -values obtained from all methods increased for both specimens. The percentage deviations of Ψ_{Nu} -values from the hot box measurements are -2% and +1% for Specimen 1 and Specimen 2, respectively. The Ψ_{Jur} -values represent slightly higher deviations, equal to -6% for the first and -4% for the second specimen. For the highest wind velocities in Case 3, the largest Ψ -values were achieved in all methods. In this case, Ψ -values obtained by means of the ITT are slightly higher than those derived from the hot box. Ψ -values based on h_{ce} calculated from the Nusselt correlation are higher by 5% for Specimen 1 and 12% for Specimen 2 than those measured by the hot box. Similarly, Ψ -values based on h_{ce} calculated from Jürges equation are higher by 3% for Specimen 1 and 9% for Specimen 2 than values obtained from the hot box. However, summarizing the results it can be

stated that Ψ -values determined by all methods maintain the same trend of increasing the heat loss via thermal bridging while increasing the wind velocity. The levels of relative deviations of the results show that the outdoor ITT method has been successfully validated against the well-established hot box experimental testing for these cases. Ψ -values obtained using two different approaches to calculating external convective coefficients, namely Nusselt and Jürges correlations, are very close to each other.

Fig. 8 shows graphically how Ψ -values, derived from three methods, for Specimen 1 and Specimen 2 are influenced by wind velocity. A power law function (Eq. (20)), with Pearson's coefficient R^2 between 0.83 and 1.00, is the best fit to describe the correlation between Ψ -values and wind velocity.

Coefficients d and e of the power law are given in Table 9 for each case.

$$\Psi = d w^e \tag{20}$$

For Specimen 1, the Ψ_{Nu} -values increase more rapidly than Ψ_{Jur} -values and hot box measurements, when the wind velocity increases. As a result, the trend line describing the relation of Ψ -values obtained from the ITT using the Nusselt correlation is steeper than those obtained from the ITT using Jürges approach and from hot the box. For Specimen 2, the Ψ -values measured by the hot box increase at a significantly lower rate when wind velocity rises than the Ψ -values obtained from the ITT, using both approaches to calculating h_{ce} .

6. Comparison of measured and standard Ψ -values

The standard Ψ -value is generally predicted by means of numerical modelling, in accordance with EN ISO 10211 [30]. This standard refers to standard boundary conditions from ISO 6946 [31], that includes an external surface heat transfer coefficient calculated for a wind velocity of 4 m/s. In order to compare the as-built performance of a thermal bridge to its numerical prediction, the measurements should be taken at the standard conditions. To compare Ψ -values measured at different construction stages, for example before and after an existing building retrofitting, they also must be taken at the standard conditions. However, it is not practical to carry out in-situ measurements only at a wind velocity of 4 m/s. In this section, the Ψ -value measured by the outdoor ITT with different wind velocities is compared to the standard Ψ s-value.

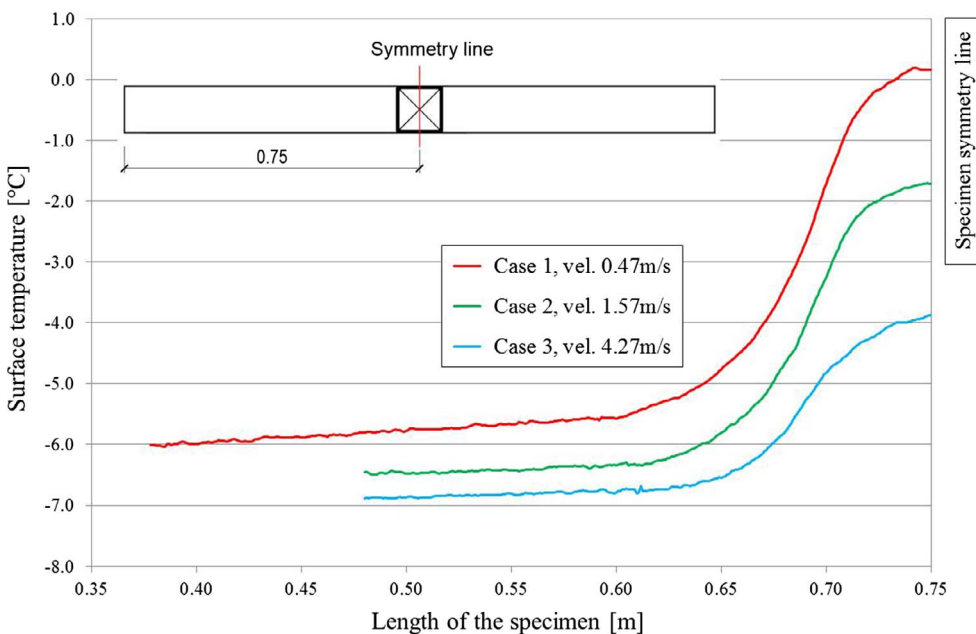


Fig. 6. The surface temperature distribution of Specimen 1 obtained with the ITT for three cases.

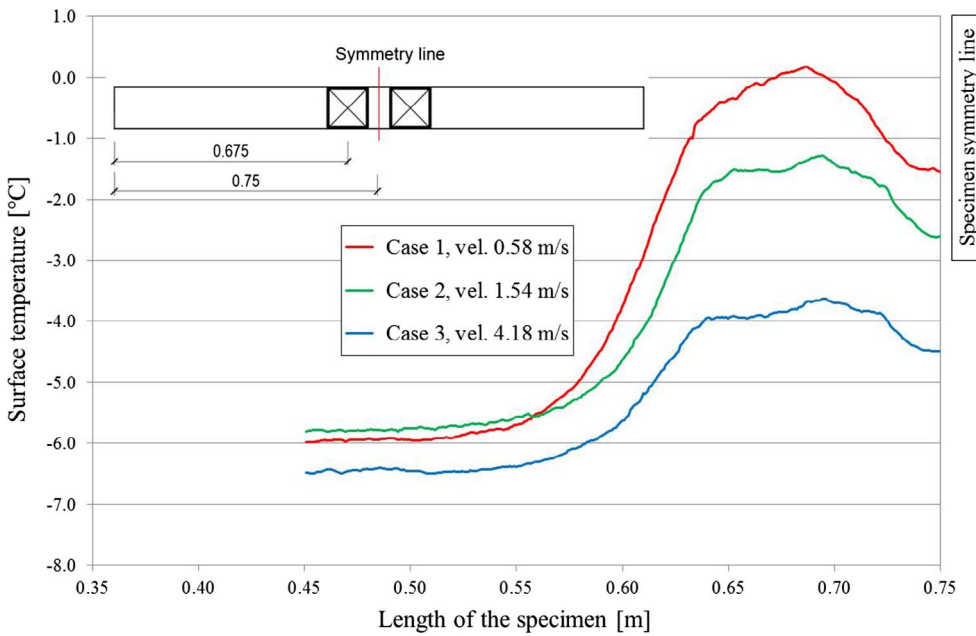


Fig. 7. Surface temperature distribution of Specimen 2 obtained with the ITT for three cases.

Table 6
Surface temperatures on the plain part T_u and on the thermal bridge T_{TB} from ITT.

Parameter	Unit	Specimen 1			Specimen 2		
		Case 1	Case 2	Case3	Case 1	Case 2	Case3
w_e	m/s	0.47	1.57	4.27	0.58	1.54	4.18
T_u (SD)	°C	-6.01 (0.08)	-6.47 (0.06)	-6.88 (0.22)	-5.93 (0.10)	-5.79 (0.07)	-6.49 (0.08)
T_{TB} (SD)	°C	0.16 (0.14)	-1.74 (0.09)	-3.88 (0.11)	0.17 (0.03)	-1.32 (0.06)	-3.63 (0.04)

Table 7
Testing conditions: the difference between air temperatures in cold and hot chambers (ΔT).

	Specimen 1			Specimen 2		
	Case 1	Case 2	Case 3	Case 1	Case 2	Case 3
	ΔT [°C]			ΔT [°C]		
Hot box	29.30	29.31	29.58	28.93	29.10	29.41
ITT	32.09	31.94	32.31	31.64	31.11	31.55
Difference	2.79	2.63	2.73	2.71	2.01	2.14

6.1. Standard Ψ -value using finite element software

In order to determine the standard Ψ -value (Ψ_s), two-dimensional heat transfer analyses were carried out for Specimens 1 and 2 using the finite element package ABAQUS. The analyses were carried out at a

Table 8
 Ψ -values obtained from the ITT using two approaches and hot box.

		Hot box	ITT Nu	ITT Ju	Hot box	ITT Nu	ITT Ju	ITT Nu/Hot box	ITT Ju/Hot box
		Ψ [W/m K]			SD [W/m K]			RD [%]	
Case 1	Specimen 1	0.243	0.220	0.231	0.020	0.004	0.004	-9.47	-4.94
	Specimen 2	0.421	0.395	0.403	0.021	0.009	0.009	-6.18	-4.28
Case 2	Specimen 1	0.253	0.249	0.237	0.010	0.020	0.019	-1.58	-6.32
	Specimen 2	0.449	0.454	0.431	0.010	0.005	0.005	1.11	-4.01
Case 3	Specimen 1	0.263	0.277	0.271	0.010	0.035	0.020	5.32	3.04
	Specimen 2	0.469	0.525	0.511	0.011	0.023	0.021	11.94	8.96

steady state and included the whole 1.5 m length of specimens. Material properties used for this simulation are presented in Table 10.

The type of element used was a 4-noded quadrilateral linear heat transfer element (DC2D). A mesh convergence study was undertaken to establish a suitable element size. An element size of 0.005 m was selected since only a 0.25% difference between total heat flow rate q_{tot} obtained with this size element and a greater size element was recorded. Because the steel post was only 0.005 m thick, a finer element size of 0.001 m was used for this part. Fig. 9 shows a portion of the mesh for Specimen 1.

The Ψ_s -values were obtained for Specimen 1 and Specimen 2 from finite numerical modelling according to the standard EN ISO 10211 [30] with standard boundary conditions recommended in ISO 6946 [31]. This standard gives different internal surface resistances R_i depending on the direction of flow in the building element considered and external surface resistance R_e calculated for wind velocity 4 m/s. These surface resistances account for radiation and convection, and their reciprocals are the standard heat transfer coefficients. For these simulations, the surface heat transfer coefficient on the internal surface of a building wall h_i was 7.7 W/(m² K) and the external surface coefficient h_e was 25 W/(m² K). The difference between indoor and outdoor air temperatures was set at 20 °C as recommended by [48]. The air temperature on the hot side was 20 °C and on the cold side 0 °C.

The simulations provide values for q_{tot} which is the total heat flow rate of the specimen per unit height. In order to determine the heat flow rate q_{TB} through a plain specimen, a similar model but without a thermal bridge was created. The difference between the heat flow rate of the specimen containing thermal bridge q_{tot} and the heat flow rate of

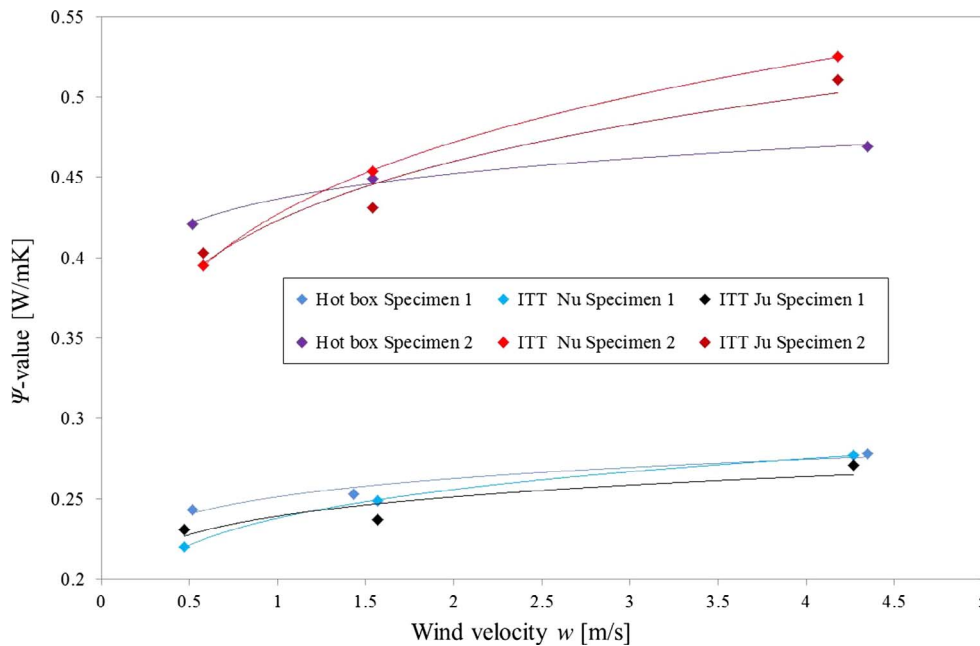


Fig. 8. Dependence of Ψ -values on wind velocity for Specimen 1 and Specimen 2.

Table 9 Values of d and e for trend lines showed in Fig. 8.

	d			e		
	Hot box	ITT Nu	ITT Ju	Hot box	ITT Nu	ITT Ju
Specimen 1	0.2512	0.2379	0.2392	0.0637	0.1043	0.0706
Specimen 2	0.4366	0.4270	0.4231	0.0509	0.1441	0.1204

Table 10 Material properties applied in 2D numerical simulation.

Property	Unit	Symbol	Material		
			OSB	Steel	XPS
Conductivity	W/m K	k	0.13 [44]	50.2 [45]	0.033 [46]
Density	kg/m ³	ρ	600 [44]	7850 [47]	33 [46]
Emissivity	–	ϵ	0.93 [19]		

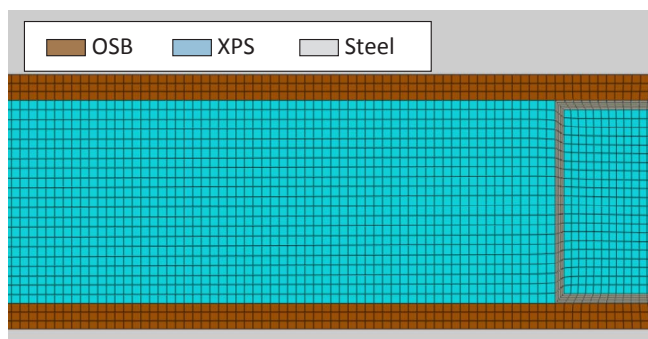


Fig. 9. A part of meshed Specimen 1.

this plain specimen q_u is the thermal bridge heat flow rate q_{TB} (Eq. (21)):

$$q_{TB} = q_{tot} - q_u \tag{21}$$

Then, the Ψ_S -value was calculated by dividing q_{TB} by the temperature difference between the hot and the cold sides in accordance with Eq. (13).

6.2. Comparison of standard and measured Ψ -values

In this section, the Ψ -values, evaluated by means of the outdoor ITT, for the two specimens, each at three wind velocities, are compared with the standard Ψ_S -values. The Ψ -values evaluated by means of the outdoor ITT using the Nusselt number correlation to determine the convective coefficient (Ψ_{Nu}) are used for this comparison. As can be seen in Table 11, the greater the difference between the test wind velocity and the standard value of 4 m/s, the greater the difference in measured Ψ -values and the standard value. For a velocity of about 0.50 m/s, the deviation from the standard value for Specimens 1 and 2 are –23% and –24%, respectively. For a wind velocity of about 1.50 m/s, the deviation is approximately –13% for both specimens. Finally, for Case 3, with a wind velocity of 4.20 m/s, the experimental Ψ_{Nu} -values show excellent agreement, with a maximum deviation of only –2% from the Ψ_S -value. Results presented in Table 11 clearly demonstrate that the thermal bridging heat losses evaluated from the ITT performed under a wind velocity lower than 4 m/s are underestimated. On the other hand, the Ψ -value obtained from the measurement taken at wind velocity in a region of 4 m/s is comparable with the standard value.

7. Adjustment of Ψ -values measured at different wind velocities to the standard values

It is not always possible to undertake a thermographic survey at the standard 4 m/s wind velocity. This section investigates how the Ψ -value obtained from the ITT undertaken at any wind velocity may be adjusted to one obtained at the standard wind velocity of 4 m/s. To examine this problem, two-dimensional heat transfer numerical simulations were

Table 11 Comparison of Ψ -value from ITT at different wind velocities to Ψ_S -value.

	Standard Ψ -value	Ψ_{Nu} -value [W/m K] obtained from:			Relative deviation (RD) from		
		ITT Case 1	ITT Case 2	ITT Case 3	Case 1/ standard	Case 2/ standard	Case 3/ standard
Specimen 1	0.284	0.220	0.249	0.277	–22.5%	–12.5%	–2.4%
Specimen 2	0.520	0.395	0.454	0.525	–24%	–12.7%	1.0%

performed. For this analysis, the range of wind velocities was extended up to 10 m/s.

The geometry of Specimen 1 was chosen for the simulations. To investigate the influence of the thermal conductivity of the main plain component surrounding thermal bridge on the Ψ -value, six different models were created where the original XPS insulation with the thermal conductivity k equal 0.033 W/(m K) for was replaced with fabric with conductivities varying between 0.05 W/(m K) and 1.00 W/(m K) as detailed in Table 12. The same steel box section used in Specimen 1 (SHS 100 × 100 × 5 mm) was the thermal bridge used in all models and the OBS facing remained unchanged.

The boundary conditions applied to finite element models were evaluated in accordance with the ISO 6946 [31]. In all cases, on the hot side, the air temperature T_i was equal to 20 °C and the sum of convective and radiative coefficient equal to 7.7 W/m² K. The air temperature on the cold side T_e was kept at 0 °C, and the convective coefficient h_{ce} was calculated for each different wind velocity using Eq. (7) in accordance to Annex A of ISO 6946 [31].

To observe the influence of the wind on the Ψ -values, all configurations (A–F) were simulated under five wind velocities: 1 m/s, 2.5 m/s, 4 m/s, 7 m/s, and 10 m/s. The results are presented in Fig. 10. The relationship between wind velocity and Ψ -value of all analyzed samples, similarly to the experimental Ψ -values shown in Fig. 8, can be described by a power law (Eq. (20)).

The power law coefficients c and b for each configuration are presented in Table 13.

In order to develop a method of adjusting the measured Ψ -value to the value evaluated at standard wind conditions, two ratios are introduced. The Ψ_{ratio} is the ratio of Ψ -value calculated for a wind velocity of 4 m/s and Ψ calculated at wind velocities other than 4 m/s. The wind ratio w_{ratio} is equal to the standard wind velocity of 4 m/s divided by the actual wind velocity at which Ψ -value was evaluated. Fig. 11 shows the relationship between Ψ_{ratio} and w_{ratio} for the six wall configurations. Fitting a power law to the data, the relationship can be written as Eq. (22) with the coefficient for each wall configuration given in Table 14:

$$\Psi_{ratio} = f w_{ratio}^g \quad (22)$$

As the value of coefficient f is approximately 1 for all samples, the expression for Ψ_{ratio} can be approximated as:

$$\Psi_{ratio} = w_{ratio}^g \quad (23)$$

Coefficient g in Eq. (23) is linearly dependent on the surface heat flux of the uniform part of the component \dot{q}_u as seen in Fig. 12.

Now the Ψ_{ratio} can be expressed by Eq. (24):

$$\Psi_{ratio} = w_{ratio}^{0.0013\dot{q}_u + 0.0525} \quad (24)$$

Knowing the wind velocity at which the Ψ -value was measured and the surface heat flux of the uniform part of the specimen, the Ψ_{ratio} can be calculated. This can then be used to adjust the measured Ψ -value to obtain the Ψ adjusted (Ψ_{adj}) to a wind velocity of 4 m/s using Eq. (25). This Ψ_{adj} can be then compared to the Ψ_S - value.

$$\Psi_{adj} = \Psi_{ratio} \Psi_{meas} \quad (25)$$

The adjustment factors are applied to the experimentally measured Ψ -values of specimens tested at different velocities to make them comparable to the standard value. To calculate the Ψ_{ratio} , the uniform surface heat flux \dot{q}_u of the component surrounding the thermal bridge is first calculated. The value of \dot{q}_u is calculated using Eq. (26), where N is the number of pixels on the IR line, and q_{xu} is calculated using Eq. (10) applied to the uniform part of the specimen away from the thermal bridge:

$$\dot{q}_u = (N * q_{xu}) / L \quad (26)$$

Values of \dot{q}_u of tested specimens for each case are given in Table 15.

Using first Eq. (24), the Ψ_{ratio} was calculated for each case and all

experimental Ψ -values (Ψ_{meas}) were multiplied by these ratios. Table 16 presents the Ψ -values obtained from the ITT at different wind velocities adjusted to the Ψ -value obtained at 4 m/s and their comparison to the standardized Ψ_S -value. As can be seen, the relative deviation between these values is significantly lower than those of non-adjusted values presented in Table 11. The relative deviation of Ψ -values measured at the lowest wind velocity around 0.5 m/s reduced from –23% and –24% before adjustment to –11% and –14% after adjustment for Specimens 1 and 2, respectively. In the next case, when the wind velocity was around 1.5 m/s the relative deviations reduced from –13% before adjustment to –7% after adjustment for both specimens. In the last case, the differences between the measured and the standard results are very small and changed insignificantly after the adjustment procedure. This occurred because Case 3 represented a wind velocity around 4 m/s and the adjustment is not necessary. The analysis also shows that the adjustment procedure is more effective when applied to Case 2 (1.5 m/s) rather than to Case 1 (0.5 m/s).

8. Conclusions

A non-destructive measurement methodology for determining the linear thermal bridge performance, using infrared thermography applied to the exterior building surface, is presented. A method of accounting for different wind velocities is proposed, which allows for measurements under different wind conditions to be adjusted to standard conditions. The methodology is evaluated by comparison with experimental measurements in a hot box device and numerical modelling of the tested components.

Key conclusions from the work are as follows:

- Heat loss from a building surface is significantly influenced by wind velocity with Ψ -values increasing with increasing velocity. Measurements of Ψ -value at a wind velocity below 4.0 m/s are lower than the standard Ψ -value. For specimens tested at ~0.5 m/s, the relative deviation is ~23%.
- Wind impacts on the heat loss through thermal bridges are significantly greater than through the plain parts of the component. For the tested components, increasing the wind velocity from ~0.5 m/s to ~4 m/s resulted in a temperature drop at the thermal bridge of 3.8 °C (Specimen 2) and 4.0 °C (Specimen 1) while the corresponding drop on the plain part of the component were only 0.6 °C and 0.9 °C.
- For the Ψ -value calculation, the external convective coefficient h_{ce} was determined using Jürges approximation and the Nusselt number. The results of this study demonstrated the suitability of both approaches for Ψ -value calculation, while Jürges approximation is less time-consuming.
- ITT is an effective tool for determination of the Ψ -value. For specimens with single and multiple thermal bridges, tested at wind speeds between 0.5 m/s and 4.0 m/s, the relative deviation between the Ψ -value determined using the proposed methodology and that from hot box measurements varied between +5% and –9%.
- Based on a numerical study, where a wide range of wall thermal conductivity values were investigated, a power law relationship was established between the Ψ -ratio (the ratio of the Ψ -value under standard wind conditions to that at other wind velocities) and the wind ratio (the ratio of the standard wind velocity of 4 m/s to the other wind velocity). The exponent of the power law is expressed as a function of the surface heat flux of the uniform part of the

Table 12
Thermal conductivity of insulation material in wall configurations A–F.

Sample	A	B	C	D	E	F
k [W/m K]	0.033	0.050	0.150	0.320	0.650	1.000

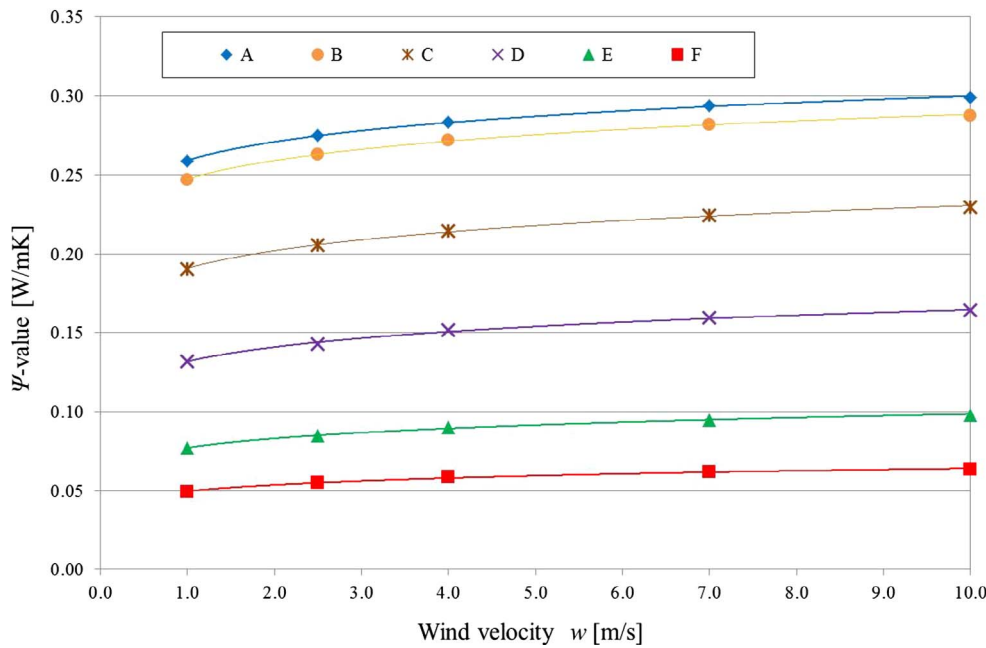


Fig. 10. Dependence of Ψ -values on wind velocity for six wall samples.

Table 13
Values of d and e for configurations A–F.

	A	B	C	D	E	F
d	0.2599	0.2480	0.1913	0.1323	0.0775	0.0499
e	0.0603	0.0636	0.0789	0.0920	0.1016	0.1068

Table 14
Coefficients f and g for Eq. (22) and uniform surface heat fluxes q_u for wall samples.

	A	B	C	D	E	F
f	1.0039	1.0043	1.0058	1.008	1.0091	1.0115
g	0.061	0.0636	0.0778	0.0920	0.1016	0.1068
q_u	5.80	8.29	21.63	28.39	36.92	41.16

specimen.

- To date, the methodology has been validated under laboratory conditions in a hot box device for a range of wind speeds up to 4.0 m/s. The test specimens were manufactured from high thermal efficiency SIP panels, which provide a very severe test of the ITT approach. The accuracy levels achieved indicate that there is great potential for widespread adoption for in-situ use on existing buildings. The adjustment procedure makes the methodology practical for application in wind conditions up to 4.0 m/s. The approach

could be implemented at different stages of a thermal retrofitting project:

- o project planning phase: to identify those building envelopes most in need of retrofitting;
- o project design phase: to determine the existing thermal performance so that an optimum retrofit strategy for each building envelope can be established;
- o project evaluation phase: to undertake a post-retrofit thermal

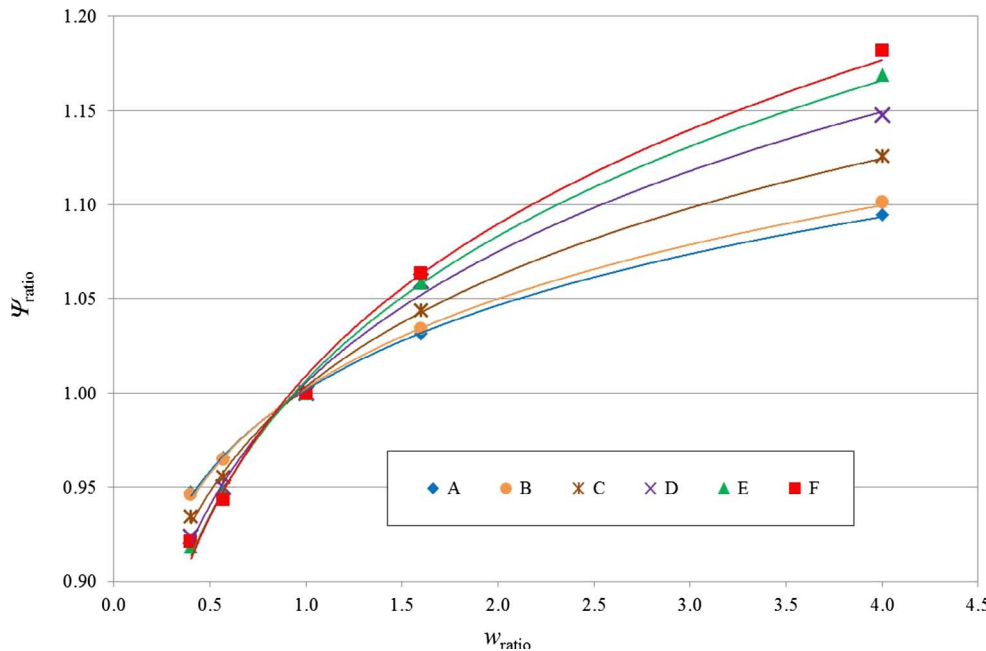


Fig. 11. Dependence of Ψ -ratio on wind ratio for six wall samples.

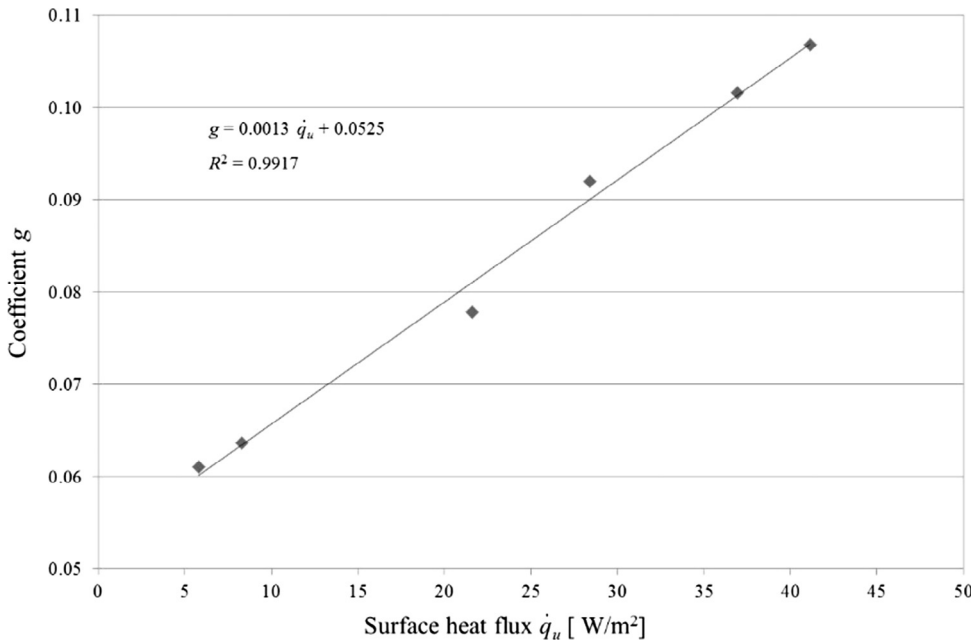


Fig. 12. Dependence of coefficient g on surface heat flux q_u .

Table 15
Uniform surface heat flux q_u of tested specimens.

	Unit	Uniform surface heat flux q_u for:		
		Case 1	Case 2	Case 3
Specimen 1	W/m ²	8.54	8.93	9.56
Specimen 2	W/m ²	8.29	8.62	9.18

Table 16
Comparison of adjusted Ψ -value to the standard Ψ -value.

	Standard Ψ -value	Ψ -value adjusted [W/m K]:			Relative deviation		
		ITT			Case 1	Case 2	Case 3
		Case 1	Case 2	Case 3			
Specimen 1	0.284	0.252	0.264	0.276	-11.2%	-6.9%	-2.9%
Specimen 2	0.520	0.446	0.482	0.524	-14.2%	-7.3%	0.8%

condition survey and demonstrate the effectiveness of the measures used and inform future design approaches.

Acknowledgments

The authors wish to thank the following
 (1) Cracow University of Technology CUT, in particular Head of the Institute Prof. Jacek Schnotale and to the technician Eng. Mariusz Rusiecki for allowing us the opportunity to use hot box facility and for providing assistance during the experimental process.
 (2) SIP Energy Ltd., Athenry Co. Galway and in particular Mr. John Moylan for providing the test specimens for experimental purposes.
 (3) Enterprise Ireland for the provision of financial support for this study through Innovation Voucher IV-2014-4203.

References

[1] Directive 2010/31/EU of the European Parliament and of the Council on the energy performance of buildings; 2010.
 [2] Evaluation of Directive 2010/31/EU on the energy performance of buildings, European Commission <[http://www.buildup.eu/en/practices/publications/evaluation-directive-201031eu-energy-performance-buildings-commission-staff-0?](http://www.buildup.eu/en/practices/publications/evaluation-directive-201031eu-energy-performance-buildings-commission-staff-0?gid=50719)

[gid=50719](http://www.buildup.eu/en/practices/publications/evaluation-directive-201031eu-energy-performance-buildings-commission-staff-0?gid=50719)> [accessed on the 27.07.2017].
 [3] Proposal for a Directive of the European Parliament and of the Council amending Directive 2010/31/EU on the energy performance of buildings; 2016.
 [4] Pisello AL, Goretti M, Cotana F. A method for assessing buildings' energy efficiency by dynamic simulation and experimental activity. *Appl Energy* 2012;97:419–29.
 [5] Yao J. Energy optimization of building design for different housing units in apartment buildings. *Appl Energy* 2012;94:330–7.
 [6] Chantrelle FP, Lahmidi H, Keilholz W, Mankibi ME, Michel P. Development of a multicriteria tool for optimizing the renovation of buildings. *Appl Energy* 2011;88:1386–94.
 [7] Karmellos M, Kiprakis A, Mavrotas G. A multi-objective approach for optimal prioritization of energy efficiency measures in buildings: model, software and case studies. *Appl Energy* 2015;139:131–50.
 [8] Niemelä T, Kosonen R, Jokisalo J. Cost-optimal energy performance renovation measures of educational buildings in cold climate. *Appl Energy* 2016;183:1005–20.
 [9] Goggins J, Moran P, Armstrong A, Hajdukiewicz M. Lifecycle environmental and economic performance of nearly zero energy buildings (NZEB) in Ireland. *Energy Build* 2016;116:622–37.
 [10] Ascione F, De Masi RF, de Rossi F, Ruggiero S, Vanoli GP. Optimization of building envelope design for nZEBs in Mediterranean climate: performance analysis of residential case study. *Appl Energy* 2016;183:938–57.
 [11] Berger J, Mendes N. An innovative method for the design of high energy performance building envelopes. *Appl Energy* 2017;190:266–77.
 [12] Lin YH, Tsai KT, Lin MD, Yang MD. Design optimization of office building envelope configurations for energy conservation. *Appl Energy* 2016;171:336–46.
 [13] Fan Y, Xia X. A multi-objective optimization model for energy-efficiency building envelope retrofitting plan with rooftop PV system installation and maintenance. *Appl Energy* 2017;189:327–35.
 [14] EN ISO 14683 Thermal bridges in buildings construction – linear thermal transmittance – simplified methods and default values; 2000.
 [15] Kylili A, Fokaides PA, Christou P, Kalogirou SA. Infrared thermography (IRT) applications for building diagnostics: a review. *Appl Energy* 2014;134:531–49.
 [16] Benkő I. Quantitative analysis of thermal bridges of structures through infrared thermograms. In: Proceedings of international conference on quantitative infrared thermography qirt 2002, Dubrovnik, Croatia. p. 203–8.
 [17] Asdrubali F, Baldinelli G, Bianchi F. A quantitative methodology to evaluate thermal bridges in buildings. *Appl Energy* 2012;97:365–73.
 [18] Bianchi F, Pisello A, Baldinelli G, Asdrubali F. Infrared thermography assessment of thermal bridges in building envelope: experimental validation in a test room setup. *Sustainability* 2014;6:7107–20.
 [19] O'Grady M, Lechowska AA, Harte AM. Infrared thermography technique as an in-situ method of assessing the heat loss through thermal bridging. *Energy Build* 2017;135:20–32.
 [20] Fox M, Goodhew S, De Wilde P. Building defect detection: external versus internal thermography. *Build Environ* 2016;105:317–31.
 [21] Albatici R, Tonelli AM, Chiogna M. A comprehensive experimental approach for the validation of quantitative infrared thermography in the evaluation of building thermal transmittance. *Appl Energy* 2015;141:218–28.
 [22] EN 13187 Thermal performance of buildings-qualitative detection of thermal irregularities in building envelopes – infrared method; 1999.
 [23] Lehmann B, Ghazi Wakili K, Frank Th, Vera Collado B, Tanner C. Effects of individual climatic parameters on the infrared thermography of buildings. *Appl Energy* 2013;110:29–43.
 [24] Albatici R, Tonelli AM. Infrared thermovision technique for the assessment of

- thermal transmittance value of opaque building elements on site. *Energy Build* 2010;42:2177–83.
- [25] Flir Systems, User's manual FLIR Bxxx series FLIR Txxx series; 2011.
- [26] Fokaides PA, Kalogirou SA. Application of infrared thermography for the determination of the overall heat transfer coefficient (U-Value) in building envelopes. *Appl Energy* 2011;88:4358–65.
- [27] Kieszonkowy przewodnik Termografa, Tesco; 2009.
- [28] Balaras CA, Argiriou AA. Infrared thermography for building diagnostics. *Energy Build* 2002;34:171–83.
- [29] EN ISO 8990 Thermal insulation – determination of steady-state thermal transmission properties – calibrated and guarded hot box; 1997.
- [30] EN ISO 10211 Thermal bridges in building construction – heat flow and surface temperatures – detailed calculations; 2007.
- [31] EN ISO 6946 Building components and building elements – Thermal resistance and thermal transmittance – Calculation method; 2007.
- [32] Moran MJ, Shapiro HN, Munson BR, Dewitt DP. *Introduction to Thermal systems engineering: thermodynamics, fluid mechanics and heat transfer*. John Wiley & Sons, Inc.; 2003.
- [33] Hens H. *Building physics – heat, air and moisture*. Berlin: Ernst & Sohn, Wiley Company; 2007.
- [34] Nusselt W, Jürges W. Die Kühlung einer ebenen wand duren einen Luftstrom (The cooling of a wall by an air flow). *Gesundheits Ingenieur* 1922;52:641–2.
- [35] Cole RJ, Sturrock NS. The convective heat exchange at the external surface of buildings. *Build Environ* 1977;12:207–14.
- [36] Palyvos JA. A survey of wind convection coefficient correlations for building envelope energy systems' modeling. *Appl Therm Eng* 2018;28:801–8.
- [37] McAdams W. *Heat Transmission*. 3rd ed. McGraw-Hill International Book Company; 1958.
- [38] Dall'O' G, Sarto L, Panza A. Infrared screening of residential buildings for energy audit purposes: results of a field test. *Energies* 2013;6:3859–78.
- [39] Emmel MG, Abadie MO, Mendes N. New external convective heat transfer coefficient correlations for isolated low-rise buildings. *Energy Build* 2007;39:335–42.
- [40] Sartori E. Convection coefficient equations for forced air flow over flat surfaces. *Sol Energy* 2016;80:1063–71.
- [41] Rowley FB, Eckley WA. Surface coefficient as affected by wind direction. *Trans ASHRAE* 1932;38:33–46.
- [42] EN ISO 12567-1 Thermal performance of windows and doors – Determination of thermal transmittance by the hot-box method – Part 1: Complete windows and doors; 2010.
- [43] Watmuff JH, Charters WWS, Proctor D. Solar and wind induced external coefficients-solar collectors. *Comptes Rendus Int d'Heliotechnique* 1977;2:56.
- [44] Product Data Sheet of Eurostrand OSB 3, E EGGER; 2009.
- [45] <http://hyperphysics.phy-astr.gsu.edu/hbase/Tables/> [accessed on the 16.01.2017].
- [46] Product Data Sheet of Styrofoam LBH-X. Dow Chemical Company Limited; 2014.
- [47] < www.engineeringtoolbox.com/metal-alloys-densities-d_50.html > [accessed on the 16.01.2017].
- [48] Ward T, Sanders C. *Conventions for calculating linear thermal transmittance and temperature factor*. IHS BRE Press; 2007.